

Supernova remnants interacting with molecular clouds: X-ray and gamma-ray signatures

Patrick Slane · Andrei Bykov ·
Donald C. Ellison · Gloria Dubner ·
Daniel Castro

Received: date / Accepted: date

Abstract The giant molecular clouds (MCs) found in the Milky Way and similar galaxies play a crucial role in the evolution of these systems. The supernova explosions that mark the death of massive stars in these regions often lead to interactions between the supernova remnants (SNRs) and the clouds. These interactions have a profound effect on our understanding of SNRs. Shocks in SNRs should be capable of accelerating particles to cosmic ray (CR) energies with efficiencies high enough to power Galactic CRs. X-ray and γ -ray studies have established the presence of relativistic electrons and protons in some SNRs and provided strong evidence for diffusive shock acceleration as the primary acceleration mechanism, including strongly amplified magnetic fields, temperature and ionization effects on the shock-heated plasmas, and modifications to the dynamical evolution of some systems. Because protons dominate the overall energetics of the CRs, it is crucial to understand this hadronic component even though electrons are much more efficient radiators and it

P. Slane
Harvard-Smithsonian Center for Astrophysics, 60 Garden St., Cambridge, MA 02138 USA
E-mail: slane@cfa.harvard.edu

A.M. Bykov
A.F. Ioffe Institute for Physics and Technology, 194021, St. Petersburg, Russia
and
St. Petersburg State Polytechnical University, St. Petersburg, Russia
E-mail: byk@astro.ioffe.ru

D. C. Ellison
Physics Department, North Carolina State University, Box 8202, Raleigh, NC 27695, USA
E-mail: don_ellison@ncsu.edu

G. Dubner
Instituto de Astronomía y Física del Espacio (IAFE), UBA-CONICET, CC 67, Suc. 28, 1428 Buenos Aires, Argentina
E-mail: gdubner@iafe.uba.ar

D. Castro
MIT-Kavli Center for Astrophysics and Space Research, 77 Massachusetts Avenue, Cambridge, MA 02139, USA
E-mail: castro@mit.edu

can be difficult to identify the hadronic component. However, near MCs the densities are sufficiently high to allow the γ -ray emission to be dominated by protons. Thus, these interaction sites provide some of our best opportunities to constrain the overall energetics of these particle accelerators. Here we summarize some key properties of interactions between SNRs and MCs, with an emphasis on recent X-ray and γ -ray studies that are providing important constraints on our understanding of cosmic rays in our Galaxy.

Keywords supernova remnants · molecular clouds · X-rays · gamma-rays

1 Introduction

Within star-forming galaxies, cold molecular material forms complex structures spanning a large range of spatial scales and densities, from giant molecular clouds (MCs) spanning tens of parsecs down to compact self-gravitating cores from which stars may form. For the most massive stars, their short lifetimes will not provide sufficient time to stray far from the molecular environments in which they were born before they undergo supernova explosions. We thus expect to find many supernova remnants (SNRs) associated with core-collapse supernovae to evolve in regions with dense MCs. Interactions with MCs can strongly impact the properties and long-term evolution of SNRs, and the distinct signatures of SNR/MC interactions can place strong constraints on this process, and on the properties of the evolving plasma. These interactions can drive shocks into the molecular material, providing distinct signatures of the interaction, and can play a role in triggering new star formation. In addition, the presence of dense gas from MC regions can play a crucial role in revealing the presence of energetic ions accelerated by SNR shocks, through the production of γ -rays.

The evolution of an SNR is arguably most readily investigated through X-ray observations. The rapid shocks heat the ambient medium and supernova (SN) ejecta to temperatures of $\sim 10^7$ K, producing thermal bremsstrahlung and line emission from which the density, ionization state, and abundances of the shocked gas can be constrained. Comparison of these derived properties with models for SNR evolution produce some of the most detailed information about the progenitor systems and their environments. At the same time, efficient particle acceleration often occurs in fast SNR shocks, resulting in X-ray synchrotron radiation in the compressed and amplified magnetic fields. The relativistic protons and electrons produced in this acceleration process can produce γ -ray emission. In particular, emission associated with the decay of neutral pions produced in proton-proton collisions can be significantly enhanced in environments with high densities, such as those in which SNRs are interacting with MCs. Thus, X-ray and γ -ray signatures from SNRs carry particularly important information on interactions with MCs.

2 Observational Signatures of SNR/MC Interactions

Resolved studies of SNRs and their associated clouds are most easily carried out for systems within the Milky Way, though with the increasing capacity of new observational facilities, the studies are rapidly extending to our neighbor galaxies, the Magellanic Clouds. In our Galaxy, molecular gas clouds account for less than one percent of the volume of the interstellar medium (ISM), yet as they are the densest part of the medium, they represent roughly one-half of the total gas mass interior to the Solar circle. This mass is distributed predominantly along the spiral arms and within a narrow midplane with a scale-height $Z \sim 50 - 75$ pc, much thinner than the atomic or ionized gas (Cox 2005). Most of the molecular gas ($\sim 90\%$) appears to be in massive structures distributed in large clumps (Giant Molecular Clouds, GMCs), filaments and condensed clumps (which are the cradle for future stars). As mentioned above, most core-collapse SNe are located close to molecular concentrations, their birth places. Therefore a large percentage of the few hundreds of observed Galactic SNRs is expected to be physically related to, and maybe interacting with, MCs.

However, to unambiguously establish whether an SNR is physically associated with a MC, removing confusion introduced by unrelated gas along the line of sight is not trivial. Several distinct criteria can be used to demonstrate a possible SNR/MC interaction. Morphological traces along the periphery of the SNRs such as arcs of gas surrounding parts of the SNR or indentations in the SNR outer border encircling dense gas concentrations can be observed in images of SNRs (see Section 3.1.1). Usually such features indicate that a dense external cloud is disturbing an otherwise spherically symmetric shock expansion. These initial signatures need to be confirmed with more convincing, though more rare, features like broadenings, wings, or asymmetries in the the molecular line spectra (Frail and Mitchell 1998), high ratios between lines of different excitation state (Seta et al. 1998), detection of near infrared H_2 or [Fe II] lines (e.g., Reach et al. 2005), peculiar infrared colors (Reach et al. 2006; Castelletti et al. 2011), or the presence of OH (1720) MHz masers (e.g., Frail et al. 1996; Green et al. 1997; Claussen et al. 1997; Hewitt et al. 2008), the most powerful tool to diagnose SNR/MC interactions. The fulfillment of one or more of these different criteria can be used to propose the existence of “definitive”, “probable” or “possible” physical interactions between an SNR and a neighboring cloud.

Once the association between an SNR and a molecular feature is firmly established, it serves to provide an independent estimate for the distance to the SNR through the observed Doppler shift of the line centroid and by applying a circular rotation model for the Galaxy.¹ Based on a combination of different techniques, Chen and Jiang (2013) presented a list of ~ 70 Galactic SNRs suggested to be physically interacting with neighboring MCs, of which 34 cases are confirmed on the basis of simultaneous fulfillment of various criteria, 11 are probable, and 25 are classified as possible and deserve more studies.

The basic tool used to investigate cases of SNR/MC interactions is the survey of the interstellar medium in a field around the SNR using different spectral lines, from

¹ The drawback of this method is that Galactic circular rotation is an approximation only valid for gas close to the Galactic disk, and for sources located inside the solar circle there is an ambiguity of two different distances producing the same radial velocity.

the cold, atomic hydrogen emitting at λ 21 cm to the dense shielded regions of molecular hydrogen (that constitutes at least 99% of the molecular gas in the Milky Way) emitting in the millimeter and infrared ranges. The most widely used proxy to track down molecular gas is CO. This molecule has a nonzero dipole moment, and radiates much more efficiently than the abundant H_2 (with no dipole moment) and can be detected easily. However, such an indirect tracer can be biased, since there can still be CO-dark H_2 gas. Recent studies conducted with the Herschel Space Observatory revealed that the reservoir of molecular gas in our Galaxy can be hugely underestimated when it is traced with traditional methods (Pineda et al. 2013). Through the detection of ionized carbon [CII] at $158 \mu\text{m}$ one can trace the envelope of evolved clouds as well as clouds that are in transition between atomic and molecular. This might help to solve the question about the real proximity between clouds and the CR accelerator in some SNRs.

In what follows we discuss different tools for exploring interactions between SNRs and MCs.

2.1 HI Emission

Since the discovery of the λ 21 cm line of atomic hydrogen more than 60 years ago, it has been shown to be the perfect tool for investigating the distribution and kinematics of the interstellar medium, revealing Galactic arms, large concentrations, arcs, and bubbles. It is, then, the basic observational resource to explore the environs of SNRs searching for candidate structures with which the SNRs may be interacting. However, because of the high abundance and ubiquity, confusion with unrelated gas along the line of sight dominates, and the detection of an HI candidate structure needs to be confirmed with other indicators that reinforce the hypothesis of association. The HI can be studied either in emission or in absorption, the latter being a very effective tool for constraining the distance to the SNR. In addition, the HI mapping of large fields around SNRs is an excellent tool to explore the history of the precursor star, for example by detecting large wind-blown bubbles around the SNRs, and to estimate the gas density of the medium where the blast wave expands.

Numerous HI studies around SNRs have been carried out using single-dish and interferometric radio telescopes. Some examples are the results presented on the Lupus Loop (Colomb and Dubner 1982), G296.5+10.0 (Dubner et al. 1986), Vela (Dubner et al. 1998b), W50 - SS 443 (Dubner et al. 1998a), Tycho (Reynoso et al. 1999), SN 1006 (Dubner et al. 2002), W28 (Velázquez et al. 2002), Puppis A (Reynoso et al. 2003), Kes 75 (Leahy and Tian 2008), IC 443 (Lee et al. 2008), and several Southern Galactic SNRs (Koo et al. 2004). Recent observations also indicate the existence of shells and super-shells around SNRs (Park et al. 2013), which are particularly useful as they permit the reconstruction of the history of the SNR progenitor, providing hints on the nature of of “dark” γ -ray sources (e.g., Gabányi et al. 2013).

2.2 Molecular Emission

As mentioned above CO studies are the most widely used tool to analyze distribution and kinematics of cold, dense clouds with high molecular content. ^{12}CO in its different excitation states and ^{13}CO lines have been surveyed over most of the sky and public data are available from the classical survey “The Milky Way in Molecular Clouds” by Dame et al. (2001)², the “FCRAO CO Survey of the Outer Galaxy” by Heyer et al. (1998)³, the “Galactic Ring Survey” by Jackson et al. (2006)⁴, or the new “MOPRA Southern Galactic Plane CO Survey” by Burton et al. (2013), among others. These public databases are an excellent starting point to search for possible SNR/MC interactions. Additionally, dedicated studies using different facilities and in different molecular transitions have been conducted towards many Galactic SNRs. The SNR IC443 is a textbook case to analyze shock chemistry, from the early work by Denoyer and Frerking (1981), to tens of works investigating the chemical and physical transformations introduced by the strong SNR shocks on the surrounding MCs (e.g., White et al. 1987; Burton et al. 1988; Wang and Scoville 1992; van Dishoeck et al. 1993). More recently, Castelletti et al. (2011) showed a comparison between very high energy γ -ray emission as detected with VERITAS (Acciari et al. 2009), with ^{12}CO J=1-0 integrated emission (Zhang et al. 2010) revealing for the first time the excellent concordance between emissions in both regimes.

An important study carried out by Seta et al. (1998) proposed that an enhanced $^{12}\text{CO}(J=2-1)/^{12}\text{CO}(J=1-0)$ ratio in the line wings is a clear signature of physical interaction. Ratios are ≥ 3 in IC443, and higher than ~ 1 in W44, which also shows broadened line profiles indicating disrupted molecular material (Figure 1, right).

Huang and Thaddeus (1986) carried out a search for possible SNR/MC associations in the outer Galaxy, within a limited region of the northern hemisphere, finding about 13 possible associations based on spatial coincidences (out of 26 SNRs investigated). More recently, Chen et al. (2013) reported CO observations towards a number of SNRs possibly interacting with MCs.

2.3 Masers

OH (1720 MHz) masers have long been recognized as signposts for SNR/MC interactions (e.g., Frail et al. 1994). This maser line is inverted through collisions with H_2 behind non-dissociative C-type shocks propagating into MCs (Frail and Mitchell 1998; Reach and Rho 1999). The conditions required for the maser formation are rather narrow, with temperatures in the range 50 – 125 K, densities between $n = 10^3 - 10^5 \text{ cm}^{-3}$, and OH column densities of $10^{16} - 10^{17} \text{ cm}^{-2}$ (Lockett et al. 1999). The large column requirement exceeds what can be produced by the slow shocks, indicating that an additional contribution is required to dissociate water into OH (Wardle 1999), possibly from X-rays from the hot SNR shell or from cosmic rays that may have been accelerated by the SNR. As the physical conditions needed

² <http://www.cfa.harvard.edu/mmw/MilkyWayinMolClouds.html>

³ <http://www.astro.umass.edu/fcrao/telescope/2quad.html>

⁴ <http://www.bu.edu/galacticring/>

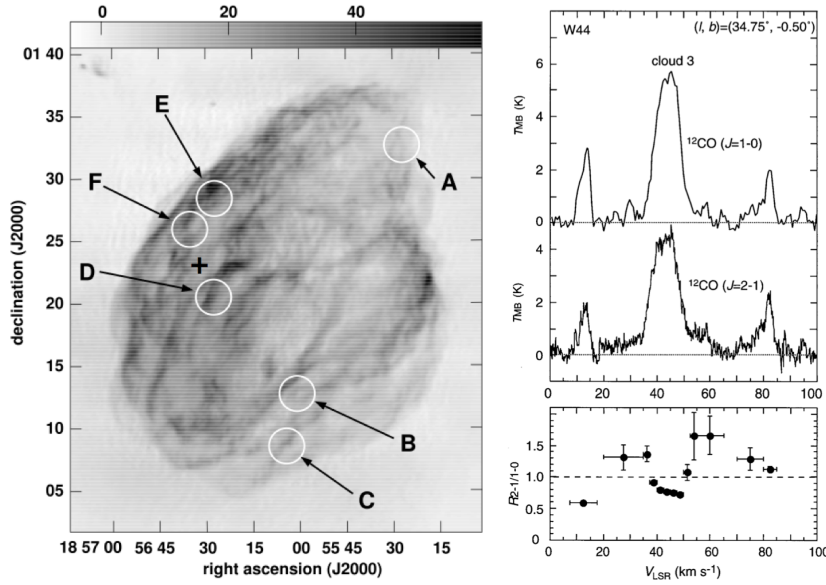


Fig. 1 Left: VLA image of W44. Circles indicate the positions of observed OH maser emission, and cross indicates the position from which the CO profile at the right is taken. Right: CO line profile from Cloud C in field of W44, illustrating broad wings produced by an interaction between the cloud and the SNR. [Left panel from Hoffman et al. 2005. Right panel from Seta et al. 1998. Reproduced by permission of the AAS.]

to pump this maser are so strict, it has to be noted that their presence is sufficient to demonstrate interaction, but its absence does not rule it out.

To date, OH (1720 MHz) masers have been found in ~ 24 SNRs, or 10% of the known SNRs in our Galaxy (Brogan et al. 2013). As summarized by Brogan et al. (2013), SNR OH (1720 MHz) masers have a large maser spot size, narrow and simple line profiles, low levels of circular polarization (less than 10%), and low magnetic field strength.

The location of masers show, in general, very good coincidence with density/shock tracers. In the case of W44 (Frail et al. 1996; Claussen et al. 1997; Hoffman et al. 2005), there is a strong correlation between the morphology of the molecular gas and the relativistic gas traced by synchrotron emission at centimeter wavelengths.

In addition to providing a clear indication of SNR/MC interactions, OH(1720 MHz) masers also permit an independent estimate for the kinematic distances to the clouds, and thus for the remnants. Also, and very important, they provide the only means of directly observing the magnetic field strength using the Zeeman effect (Brogan et al. 2000, 2013).

2.4 Radiative shocks

The evolution of supernova shells colliding with MCs differs from SNRs expanding in a pre-supernova wind or of those expanding in a homogeneous uniform ISM

(Chevalier 1999). Observations have revealed that MCs are complex structures with a hierarchical structure of dense clumps embedded in an inter-clump gas of moderate density ~ 10 H atoms cm^{-3} . The volume filling factor of the dense clumps is typically a few percent and the clump mass ranges from a fraction of M_{\odot} to thousands of M_{\odot} . The total mass in the clumps can be comparable or more than the mass of the inter-clump gas.

The dense MC environment results in an early end of the adiabatic phase of the SNR expansion. An SNR leaves the adiabatic phase and enters the *pressure driven snowplow* (PDS) stage which eventually results in the formation of a radiative shell at an age estimated by Cioffi et al. (1988) to be $\tau_{\text{sf}} = 3.6 \times 10^4 E_{51}^{3/14} n_{10}^{-4/7} \zeta_m^{-5/14}$ years, where E_{51} is the kinetic energy of supernova shell in units of 10^{51} erg, n_{10} is the ambient number density in units of 10 cm^{-3} , and ζ_m is a metallicity factor of order 1 for solar abundances. Note that the transition of the SNR to the PDS stage is expected to occur somewhat earlier than τ_{sf} . The shock radius and velocity at the beginning of the PDS stage are $R_{\text{pds}} = 5.2 E_{51}^{2/7} n_{10}^{-3/7} \zeta_m^{-1/7}$ pc and $v_{\text{pds}} = 573 E_{51}^{1/14} n_{10}^{1/7} \zeta_m^{3/14}$ km s^{-1} correspondingly. Chevalier (1999) noted that a power law expansion in time is a reasonable approximation for the radiative shell over a range $(5-50)\tau_{\text{pds}}$.

Radiative shocks in evolved SNRs are characterized by the efficient cooling of the post-shock plasma by line radiation from the dense shell behind the collisionless shock transition. The structure of the radiative shock depends on the line opacity which, for radiative SNR shocks, typically allows the escape of some optical and fine-structure infrared (IR) lines of abundant ions providing observational diagnostics of the shocks (see e.g., Raymond 1979; Hollenbach and McKee 1989; Gnat and Sternberg 2009; Bykov et al. 2013a).

In the case of core-collapse supernovae in such MC environments, the remnant becomes radiative at a radius of $\lesssim 6$ pc, forming a shell that is magnetically supported and whose structure can be described by a self-similar solution (Chevalier 1999). The expected structure of the radiative shell is illustrated in the left panel in Fig. 2. The interaction of the radiative shell with an ensemble of molecular clumps of different sizes, masses, and cloud magnetization in the model results in both J and C-type shocks with a range of velocities. In some cases, OH maser emission may be associated with shocked molecular clumps. For IC 443, for example, Snell et al. (2005) detected the shocked clumps B, C, and G in H_2O , ^{13}CO , and C I line emission with *Submillimeter Wave Astronomy Satellite* (SWAS) detectors. They concluded that, to explain these observations, different type shocks with a range of velocities is likely required. Recently, Lee et al. (2012) found observational evidence for shocked clumps by mapping the southern part of IC 443 with ^{12}CO J = 1-0 and HCO+ J = 1-0 lines.

Radiative shocks are observed in the northeast part of the SNR IC 443 where it is very likely interacting with an HI cloud. Spectrophotometry of [O III], [N II], and [S II] optical line emission performed by Fesen and Kirshner (1980) is found to be consistent with a radiative shock propagating in an inhomogeneous ISM. Electron densities up to 500 cm^{-3} were derived from the [S II] lines measurements. Kokusho et al. (2013) presented the near-IR [Fe II] $1.257 \mu\text{m}$ and [Fe II] $1.644 \mu\text{m}$ line maps ($30' \times 35'$) of IC 443 made with *IRSF/SIRIUS*. They found that [Fe II] filamentary

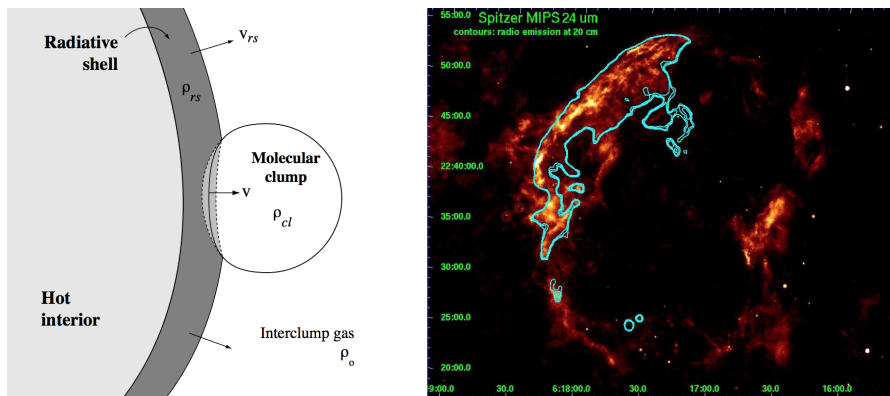


Fig. 2 Left: The sketch illustrating the interaction of the radiative supernova shell with a clumpy MC as described by Chevalier (1999). Right: *Spitzer MIPS* 24 μm image of IC 443 SNR with 1.4 GHz radio contours from Bykov et al (2008). The radiative shock is located in the northeast part of the remnant.

structures exist all over the remnant, not only in the ionic shock NE-shell, but also in a molecular shock shell and a central region inside the shells.

Earlier, *Two Micron All Sky Survey (2MASS)* images of the entire IC 443 remnant in near-IR J (1.25 μm), H (1.65 μm), and Ks (2.17 μm) were analyzed by Rho et al. (2001) who revealed some clear morphological differences between the northeastern and southern parts. The J- and H-band 2MASS emission from the NE rim was attributed mostly to different ionic fine-structure lines, where the H-band is often dominated by [Fe II] 1.644 μm line emission. The 2MASS emission in the K_s-band with 2.12 μm H₂ molecular line emission, indicated a shocked molecular ridge spanning the southern region due to interaction of the remnant with the adjacent MC.

In the right panel of Fig. 2 we show the *Spitzer MIPS* 24 μm image of IC 443 SNR taken from Bykov et al. (2008) with 1.4 GHz radio contours. The 24 μm emission is likely dominated by [Fe II] 26 μm line emission rather than by the heated dust. This was first established by Oliva et al. (1999) who showed, using *ISO-SWS* spectroscopy, that most of the 12 μm and 25 μm band *IRAS* flux is accounted for by the line emission from [NeII] and [FeII] rather than dust emission. Apart from the [Fe II] 26 μm line, the other fine-structure far-IR lines [OI] 63.2 μm and [C II] 157.7 μm are predicted to be bright in the radiative shock models of Raymond (1979) and Hollenbach and McKee (1989). Indeed, Reach & Rho (1996) estimated the luminosity of W44 in [OI] 63 μm line emission to be about 4×10^{36} erg s⁻¹, which Chevalier (1999) argued was consistent with the radiative shock models.

For the densities inferred for IC 443, the radiative shell is expected to form when the forward shock velocity drops below $v_{\text{pds}} \sim 600$ km s⁻¹. For shock speeds $> v_{\text{pds}}$, efficient diffusive shock acceleration (DSA) can occur and a substantial fraction of the shock ram pressure can be transferred into relativistic particles and turbulent magnetic fields which may be amplified to values well above those expected from adiabatic compression alone. The filamentary line emission region in the NE part of IC 443 is clearly correlated with the bright 1.4 GHz radio emission shell. This is an indication of the particle acceleration process in the shock. In contrast to the

value of $v_{\text{pds}} \sim 600 \text{ km s}^{-1}$, the radiative shock velocity in the NE shell of IC 443 was estimated to be about 100 km s^{-1} , while W44 is likely expanding at 150 km s^{-1} . It must be noted however, that these estimates were based on line emissivity derived in radiative shock models which did not account for efficient CR acceleration in the shocks. Particle acceleration, and the escape of high-energy CRs, result in higher compression and lower post-shock temperature at a given shock velocity than predicted ignoring DSA. The effect of CR acceleration on the line luminosity and ratios was discussed by Bykov et al. (2013a) who found a rather strong sensitivity of the line ratios to the extra shock compression effect. This implies the need for self-consistent models of radiative shocks including the efficient production of a non-thermal components.

3 X-rays from SNR/MC Interactions

As a young SNR evolves, it compresses and heats the surrounding medium to X-ray emitting temperatures. Where the medium is extremely dense, however, the shock velocity is slow and the temperature of the shocked plasma can be considerably lower. In addition, the expansion of the remnant can be significantly impeded, leading to a distorted morphology. The high density can lead to rapid ionization, and can also drive a strong reverse shock into the ejecta. The X-ray characteristics thus provide important signatures of SNR/MC interactions.

3.1 Morphological Effects

In the Sedov phase of evolution, the radius of an SNR at a given age scales as $R_{\text{SNR}} \propto n_0^{-1/5}$. Despite this weak dependence, variations in density of a factor of five will produce significant changes in the remnant size of about 40% and can easily cause noticeable modifications to the remnant shape. Molecular cloud environments are characterized by significant variations in density, and the clouds themselves have densities nearly $10^2 - 10^3$ times higher than that of the typical ISM. SNR evolution in such environments can thus lead to deviations from the spherical morphology expected under ideal evolution in a uniform medium.

In addition, the *apparent* morphologies of SNRs can depend upon the density and distribution of foreground material, through energy-dependent absorption. The transmission of the ISM to X-rays for example, is $e^{-\sigma N_H}$ where σ is the photoelectric absorption coefficient and N_H is the column density of gas. Hydrogen itself does not produce significant absorption at X-rays energies. Rather, N_H acts as a tracer of other atoms with K-shell and L-shell transition energies in the soft X-ray band ($\sim 0.1 - 10 \text{ keV}$), given some relative abundance distribution relative to H. This has two significant effects on X-ray images of SNRs. First, for large values of N_H associated with large distances through the ISM, the observed X-ray emission will be faint. Second, the presence of MCs along the line of sight to an SNR will produce excess absorption. This can result in complete absorption from particular regions of the SNR, changing its apparent morphology. Because the absorption coefficient

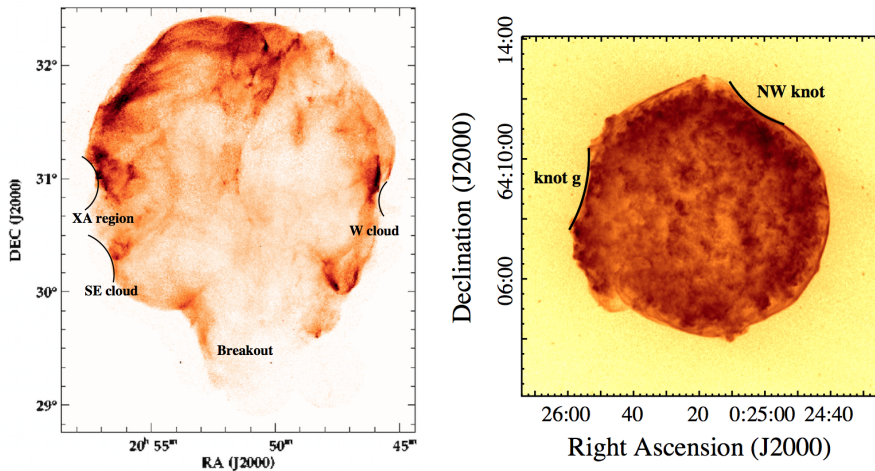


Fig. 3 Left: ROSAT HRI image of Cygnus Loop. Distinct deformation of the shell is seen at positions of cloud interactions indicated by arcs. Right: *Chandra* image of Tycho’s SNR. Arcs in the east (so-called “knot g”) and northwest indicate positions of cloud interactions.

increases rapidly at low energies (e.g., Morrison and McCammon 1983), comparison of the morphology in low and high energy bands can reveal evidence for foreground MCs. Equivalently, spectral analysis of different regions of the SNR can reveal excess absorption of soft photons in the regions along the line of sight to MCs.

3.1.1 Shell Deformation

The complex CSM/ISM structure surrounding many SNRs, often characterized by significant large-scale density gradients, can result in very significant deviations from a circular morphology (e.g., Lopez et al. 2009). Direct interactions with dense clouds can also modify the morphology of SNRs, causing distinct deformation of the shell-like structure. In Figure 3 (left) we show the ROSAT HRI image of the Cygnus Loop (Levenson et al. 1999), a nearby middle-aged SNR. The SNR shell is roughly circular, but significant deviations from circularity are seen in four regions. In the south, there is an apparent breakout associated with evolution into a low-density region. In the west, and in two positions in the east, there are very distinct arc-like deformations known as the W knot, the SE knot, and knot XA. The SE knot represents an encounter of the SNR blast wave with a protrusion from a large cloud. X-ray emission interior to radiative filaments in this region appears to originate from the reverse shock produced in the interaction (Graham et al. 1995). Knot XA appears to correspond to a dense, clumpy region resulting from an interaction with the wall of a cavity swept out by a precursor wind (McEntaffer and Brantseg 2011).

Also shown in Figure 3 is a *Chandra* image of Tycho’s SNR (right). While the overall morphology of this young, ejecta-dominated, historical remnant (SN 1572) is fairly circular, there are obvious depressions in the northwestern and eastern regions (indicated with arcs in the Figure). Density estimates based on the IR emission from

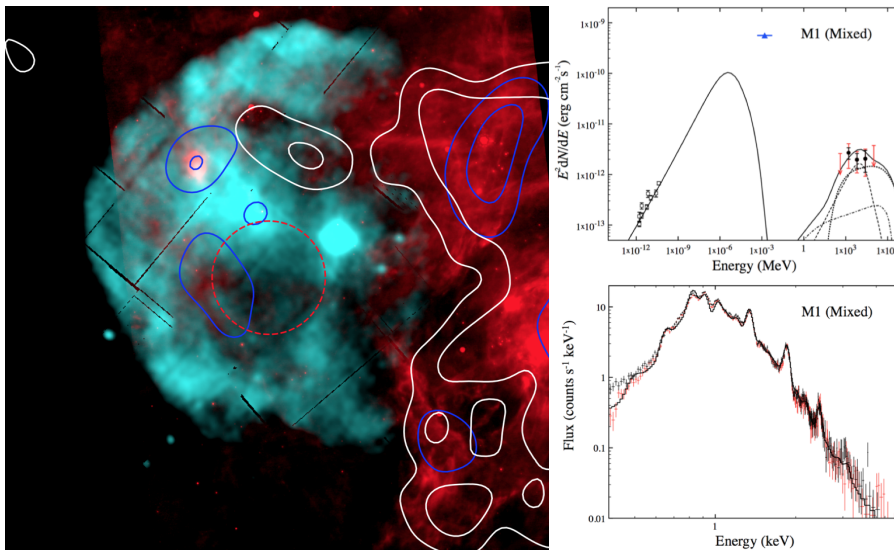


Fig. 4 Left: *XMM-Newton* image of CTB 109 (cyan) with *Spitzer* MIPS 24 μm image of adjacent MC (red). The white (blue) contours correspond to the CO line emission as observed by the CGPS, at velocity -51 (-54) km s^{-1} , and the levels correspond to 0.5 and 1.5 K. The 95% confidence radius of the centroid of the associated Fermi-LAT source is shown as a dashed red circle. Right: Broadband emission model for CTB 109 (top) and thermal X-ray emission fit to predictions of broadband model (bottom). [Figures from Castro et al. 2012. Used by permission of the AAS.]

the remnant shell reveal dramatic increases in these regions (Williams et al. 2013), and X-ray proper motion measurements show that the expansion rate is lower in these regions than for adjacent regions of the remnant (Katsuda et al. 2010). These observations are consistent with the interpretation that Tycho is encountering dense clouds in the east and northwest, and optical studies of knot g, located in the eastern limb depression, show direct evidence of radiative shocks from the interaction.

A much more dramatic example of an SNR/MC interaction is that of CTB 109. As shown in Figure 4 (left), the X-ray emission (cyan) is characterized by a half-shell morphology, with the western half of the SNR completely missing. CO measurements reveal a massive MC in this western region (white contours) from which IR emission is also seen (red image, from *Spitzer*). Radio observations at 1420 MHz show the same half-shell morphology (Kothes et al. 2002), confirming that the missing X-ray emission in the west is not produced by excess absorption. Rather, upon encountering the massive cloud, the SNR shock has apparently completely stalled.

A different approach was very recently adopted by Miceli et al. (2014), where the authors demonstrated the connection between shock-cloud interactions and particle acceleration in the southwestern limb of the historic remnant of SN 1006 based on the comparison of X-ray data with HI data. Figure 5 shows the X-ray image of the SW part of SN1006 in the 0.3-2 keV band with HI contours superimposed. Exactly at the position where an indentation is observed in the X-ray (and radio) limb, there is an HI cloud. The existence of enhanced density was also confirmed by other means by (Winkler et al. 2014). Several lines of evidence indicate that at this site particle

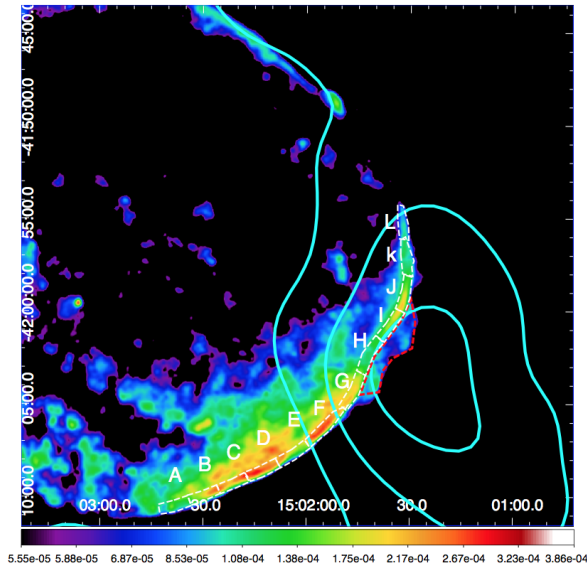


Fig. 5 *XMM-Newton* image of the southwestern portion of SN 1006 in the 0.3-2 keV band with HI column density plotted in contours showing the presence of a neutral gas cloud perfectly fitting the concavity in the SNR limb (Figure from Miceli et al. 2014).

acceleration is highly efficient and there is shock/cloud interaction, thus making this site a very promising source of γ -ray hadronic emission likely to be detectable with the *Fermi* LAT in the near future.

3.1.2 Mixed Morphology

A distinct subclass of remnants, known as mixed morphology (MM) SNRs, is characterized by a typical shell-like radio morphology contrasted by a centrally-bright X-ray morphology in which the central emission is thermal in nature (Figure 6, left). At present, there are ~ 40 known MM SNRs (see summary by Vink 2012), but the nature of the central X-ray emission is poorly understood. While abundance determinations from X-ray spectra indicate evidence for the presence of ejecta in some such remnants (e.g., Shelton et al. 2004; Lazendic and Slane 2006; Bocchino et al. 2009; Pannuti et al. 2010; Yamaguchi et al. 2012), the estimated mass of X-ray emitting material in the central regions is generally much too high to be composed primarily of ejecta.

The spectral properties in MM SNRs provide significant constraints on the evolution of these systems. The plasma appears to be nearly isothermal in many systems, quite in contrast to the temperature profile expected in the Sedov phase of evolution. In addition, recent studies have shown that the plasma is overionized in several MM SNRs (see Section 3.2.2). This may result from early evolution through a dense wind profile created during the late phase of a red supergiant (or perhaps Wolf-Rayet) progenitor. In this scenario, the plasma is quickly ionized as the shock passes through

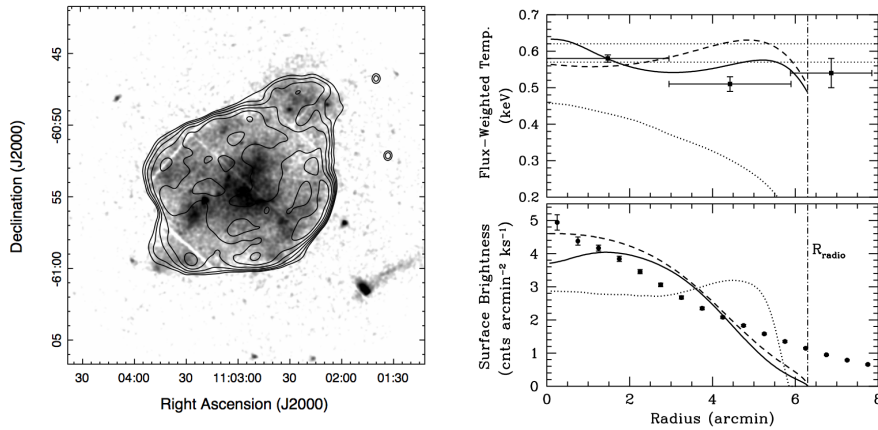


Fig. 6 Left: *XMM-Newton* image of MSH 11–61A with radio contours from MOST. The centrally-dominant emission is thermal in nature, and characterizes this as a MM SNR. Right: Brightness (bottom) and temperature (top) distributions for MSH 11–61A along with predictions from cloudy ISM (solid, dashed) and thermal conduction (dotted) models (after Slane et al. 2002). Horizontal lines in upper panel indicate mean temperature range.

the dense wind, but rapidly cools when the shock breaks through into the lower density surroundings, leaving the plasma in a higher ionization state than expected for its temperature (Moriya 2012). It is not clear exactly how such a scenario also leads to a centrally-bright morphology at later stages, nor have detailed models for such a scenario been carried out to confirm that a sufficient amount of material is shocked at this early stage to persist as an observable overionized feature in late stages of evolution.

Early models for MM SNRs centered primarily on two scenarios. In one, evolution to the radiative phase in which the shell temperature drops to low temperatures allows interstellar absorption to reduce the observed emission from the shell, while thermal conduction while the remnant is young and hot results in the transport of heat and bulk material into the central regions, smoothing out the temperature profile and increasing the emission from the remnant center (Cox et al. 1999). Application of this model to W44 is able to reproduce some general features, but fails to fully explain both the temperature and brightness distributions observed for this remnant (Shelton et al. 1999).

A second scenario centers on evolution in a surrounding medium filled with dense clouds (White and Long 1991). Upon being overtaken by the expanding SNR, the clouds evaporate through saturated conduction in the hot remnant interior, slowly increasing the central emission. For different combinations of the cloud evaporation timescale and the ratio of the mass in clouds to that in the intercloud material, significantly peaked brightness profiles can be obtained. Applying this model to the emission from MSH 11–61A, Slane et al. (2002) found that reasonable agreement could be obtained for both the radial brightness and temperature distributions (Figure 6, right), but that the required evaporation timescale ($\sim 10 - 40$ times the age of the remnant) appears much longer than expected. Application of the thermal-

conduction/radiative-phase scenario was unable to reproduce the temperature and brightness distributions.

Importantly, the vast majority of MM SNRs appear to be interacting with MCs, and nearly half are observed to produce γ -ray emission, providing an additional clue as to the conditions that lead to the observed properties. At this stage, though, MM SNRs remain poorly understood. At the same time, increases in our knowledge of the abundance, ionization, and thermal properties of the shocked central plasma offer promise for constraining more complete models of these systems.

3.2 Spectral Signatures

The temperature, composition, and ionization state of the shocked gas in an SNR all depend crucially on the properties of the medium into which the remnant evolves. In particular, dense environments associated with the presence of MCs can produce spectral signatures that reveal the SNR/MC interactions. Such signatures are readily observed in a host of individual remnants.

3.2.1 Temperature and Absorption Variations

As an SNR sweeps up excessive amounts of material in the dense regions around a MC, the shock velocity drops. If the MC interaction is confined to only discrete regions in the SNR, this can result in temperature variations in the shocked plasma. X-ray studies of W51C (Koo et al. 2002, 2005) reveal a $\sim 20\%$ temperature decrease in the northern regions where the SNR is interacting with a MC. Spectral modeling also indicates an increase in the column density, N_H , in this region, suggesting that a portion of the MC lies between the remnant and observer.

X-ray studies of 3C 391 also reveal N_H variations associated with a MC interaction, here in the northwestern regions of the remnant (Chen and Slane 2001). The increase of $\sim 5 \times 10^{21} \text{ cm}^{-2}$ indicates a molecular cloud density of $\langle N(H_2) \rangle \sim 100 l_{pc} \text{ cm}^{-3}$ where l_{pc} is the depth, in pc, of the MC region residing in front of the SNR.

3.2.2 Ionization Signatures

Due to the high densities for SNRs encountering MCs, one expects the shocked plasma to quickly reach ionization equilibrium. This is indeed observed in some remnants. For example, along the northeast limb of W28, Nakamura et al. (2014) find that the plasma is in collisional ionization equilibrium (CIE), with signs of density variations from region to region. In the central regions of the remnant, radiative recombination continuum (RRC) features of He-like Si and S are observed (Sawada and Koyama 2012), indicating a recombining plasma. Further, excess emission near the $K\alpha$ lines of He-like Mg and Ne indicate different ionization temperatures for different elements.

Such overionization states are also observed in several other SNRs for which MC interactions occur. IC 443 shows an enhanced intensity ratio for H-like to He-like

Si, indicating an overionized plasma (Kawasaki et al. 2002), and also distinct RRC features (Yamaguchi et al. 2009), for example. RRC features are also observed for W44, which also shows enhanced emission from H-like Si (Uchida et al. 2012), and from W49B (Ozawa et al. 2009). Interestingly, the nature of such overionized plasmas may actually be only indirectly associated with the presence of MCs. Although thermal conduction has been suggested as a mechanism by which heat flow from the hot SNR interior to regions with cold clouds could bring lower the electron temperature to values below the current ionization temperature of the ions, most calculations indicate that this process is too slow to operate efficiently in the typical lifetime of an SNR (e.g., Uchida et al. 2012). Instead, early evolution through a dense medium such as that from a stellar wind may have created a high ionization state, with subsequent rapid cooling as the remnant expands adiabatically into a low density cavity leading to a temperature that is lower than the ionization temperature (e.g., Yamaguchi et al. 2009; Uchida et al. 2012; Moriya 2012). Maps of the ionization state in W49B indicate higher states of overionization in the central and western regions (Miceli et al. 2010; Lopez et al. 2013), supporting the notion that rapid expansion in the direction opposite that of a dense MC in the east is responsible for the cooling.

Given the above scenario, it would seem that the most direct connection between recombining plasma in SNRs and their association with MCs is simply that the proposed early-phase evolution through a dense stellar wind implies a massive progenitor star, and the remnants of such stars are often found near the molecular cloud complexes from which they formed. However, it also appears that the overionized SNRs are all of the mixed morphology class. Whether or not the overall temperature, ionization, and brightness properties of this class require specific contributions from MC interactions remains unknown, at present, but is an area of active study.

3.3 Abundances and Nonthermal Emission

In evolved remnants that have undergone considerable interactions with MCs, the total swept-up mass can be very large. If the shock velocity in the dense interaction regions is low, much of this material will be too cool to produce X-rays. However, in many systems the X-ray emitting mass, M_x , is also large. Modeling of the emission from W44 indicates roughly $100M_\odot$ of hot gas in the remnant interior (Shelton et al. 2004), for example. The roughly solar abundances for this swept-up material will thus act to severely dilute the enhanced abundances of any (much smaller) ejecta component. Nonetheless, traces of ejecta appear common in many mixed morphology remnants (e.g., Slane et al. 2002; Shelton et al. 2004; Lazendic and Slane 2006; Bocchino et al. 2009), virtually all of which appear to be interacting with molecular clouds. In IC 443, a distinct ring-like structure of hot (~ 1.4 keV) plasma with significantly enhanced abundances of Mg and Si is observed in the vicinity of a MC interaction region, suggesting that a strong reverse shock produced in this interaction with dense material has produced enhanced ejecta emission (Troja et al. 2008).

Evidence for ejecta in IC 443 also exists in the form of compact knots of X-ray emitting material (Bocchino and Bykov 2003). The observed hard spectra and enhanced abundances suggest that these may be fast-moving knots of ejecta traveling

into dense molecular material and producing $K\alpha$ emission accompanied by nonthermal bremsstrahlung (NTB) emission from shock-accelerated electrons (Bykov 2002). Knots with similar spectral properties are observed in Kes 69 and are coincident with CO emission from a nearby MC (Bocchino et al. 2012), reinforcing this interpretation. Discrete X-ray knots directly along the SNR/MC interaction region in 3C 391 are also observed (Chen et al. 2004), but while the inferred density for these knots is high, consistent with structures being driven into clouds, the abundances do not show strong evidence for metal enhancements. We note that a complete analysis of the composition of cold, dense, metal-rich ejecta from X-ray observations needs to also account for the resonant photo-absorption effect.

Regions of *low* abundance plasma have also been observed in some regions of SNRs interacting with MCs. The Fe abundance appears to be subsolar in some bright knots in W44. The abundances of other elements in these knots appear to be enhanced, possibly indicating a scenario in which ejecta fragments are traveling through MC material in which some Fe remains condensed onto dust grains (Shelton et al. 2004). In W28, the emission from the bright northeast rim that is adjacent to a MC is best described by a high density plasma in CIE with subsolar abundances of refractory elements (Nakamura et al. 2014), but in this case the abundances of volatile elements are also subsolar, complicating any interpretation of condensation onto dust grains in MC material. Similar depletions of N, O, and Ne are observed in the XA region of the Cygnus Loop (McEntaffer and Brantseg 2011).

4 Gamma-rays from SNR/MC Interactions

4.1 Particle Acceleration in SNRs

Particle acceleration in SNRs has long been suggested as a major contributor to the cosmic ray population, at least up to the knee in the spectrum at $\sim 10^{15}$ eV. The generally assumed mechanism is DSA, where some particles scatter off of self-generated turbulence and are returned to the shock region multiple times. In nonlinear DSA, a non-negligible fraction of the electrons and ions at the forward shock (FS) can reach ultrarelativistic energies. Diffusive shock acceleration has received considerable attention, and specific predictions of the nonlinear theory include (e.g., Blandford and Eichler 1987; Malkov and Drury 2001a; Bykov et al. 2013b): (i) accelerated particles obtain enough pressure to modify the shock structure, with the shock developing an extended upstream precursor; (ii) the overall shock compression ratio can increase above the Rankine-Hugoniot value of four for strong shocks, while simultaneously the subshock compression, which is mainly responsible for heating the unshocked plasma, decreases below the Rankine-Hugoniot value; (iii) the particle power law expected from test-particle DSA becomes concave, with the highest energy particles developing a spectrum harder than the test-particle power law; (iv) a significant fraction of the highest energy particles can escape from the shock, adding to the nonlinear nature of the mechanism; and (v) the production of superthermal particles goes hand-in-hand with the production of magnetic turbulence, and strong magnetic field amplification can occur in high Mach number shocks.

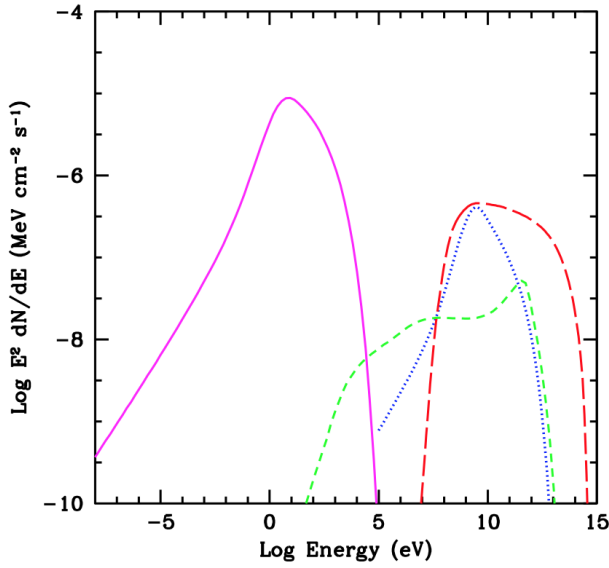


Fig. 7 Simulated broadband spectrum from SNR undergoing efficient DSA of electrons and protons. The solid magenta curve represents synchrotron emission, the dotted blue curve is IC emission, the dashed green curve corresponds to NTB, and the long-dashed curve represents the π^0 -day emission.

While there is no direct evidence for the specific mechanism of DSA in the forward and reverse shocks of SNRs, there is overwhelming evidence for the production of relativistic particles, either ions or electrons, at the forward shocks in a number of remnants. There is also clear evidence for magnetic field amplification, and for the modification of the plasma hydrodynamics, predicted by efficient DSA, in several remnants (e.g., Patnaude and Fesen 2007; Uchiyama et al. 2007; Cassam-Chenaï et al. 2008; Uchiyama and Aharonian 2008). This, combined with the direct evidence for efficient DSA in spacecraft observations of heliospheric shocks (e.g., Ellison et al. 1990) and confirmation of fundamental aspects of the theory from particle-in-cell (PIC) simulations (e.g., Ellison et al. 1993; Sironi et al. 2013), has added to a general acceptance of the mechanism for cosmic ray production in SNRs.

Despite the progress made in understanding DSA and verifying some of its basic predictions, important open questions remain about the maximum particle energy E_{max} , the acceleration efficiency, the electron-to-proton ratio K_{ep} for the injected particles, and the eventual escape of cosmic rays from the acceleration region. As an example, local cosmic ray measurements, as well as theoretical expectations, suggest that shocks put far more energy in protons and heavier ions than in electrons. Yet the nonthermal emission from most astrophysical sources is dominated by radiation from relativistic electrons. While this can be understood, in part, because relativistic electrons radiate more efficiently than protons, the underlying energy budget of a source cannot be determined until constraints on the hadronic component are obtained and

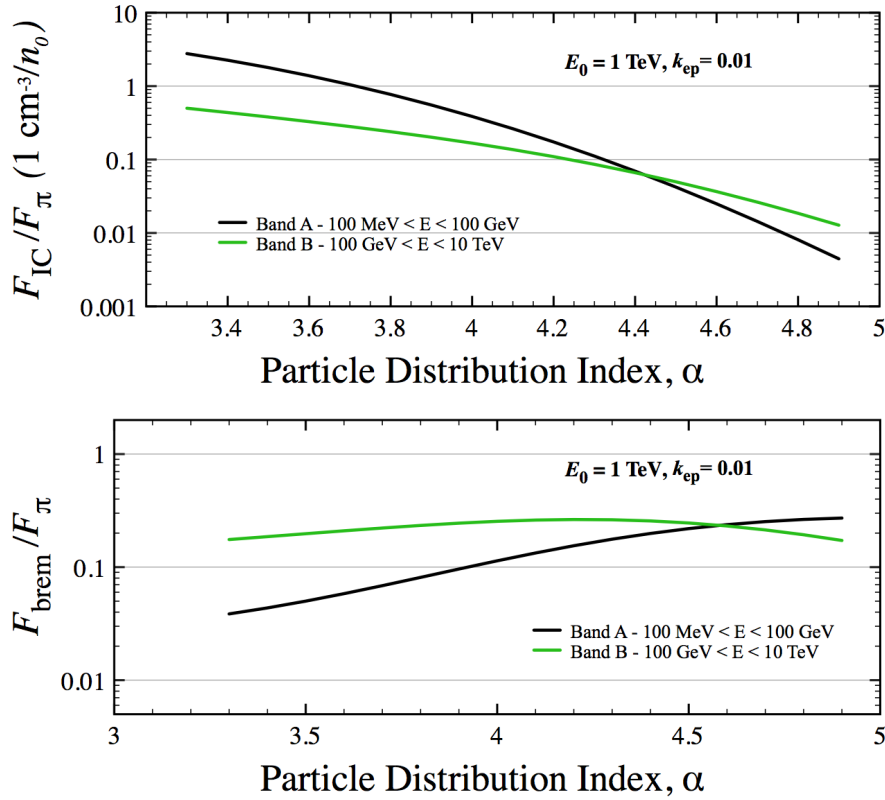


Fig. 8 IC-to- π^0 -decay (top) and NTB-to- π^0 -decay (bottom) flux ratios as a function of the particle momentum distribution spectral index, α . The black curve is for the photon energy band 100 MeV to 100 GeV, and the green line indicates the flux ratio in the 100 GeV to 10 TeV range. The exponential particle energy cutoff, for both electrons and protons, has been fixed at 1 TeV, and the electron-to-proton ratio is $K_{ep} = 0.01$. [From Castro et al. 2013. Reproduced by permission of the AAS.]

the accelerated electron-to-proton ratio determined. This is important for cosmic rays and for all sources where DSA is expected to occur.

Molecular clouds play a particularly important role in this regard because shocks in the high density MC environment will predominately produce γ -rays by hadronic interactions rather than leptonic ones (e.g., Aharonian et al. 1994).

4.2 Gamma-ray Production

Gamma-ray production from such relativistic particles can proceed through inverse-Compton (IC) scattering of ambient photons by the energetic electrons, nonthermal bremsstrahlung (NTB) from collisions between relativistic electrons and ambient material, and the decay of neutral pions formed in collisions of energetic protons with surrounding nuclei. Figure 7 presents a simulation of the broadband spectrum pro-

duced by an SNR undergoing efficient acceleration of electrons and ions. The magenta curve represents synchrotron emission from the relativistic electrons, and the dotted blue curve corresponds to IC emission produced from that same electron population up-scattering photons from the cosmic microwave background (CMB). The dashed green curve represents NTB from the relativistic electrons interacting with ambient material, and the long-dashed red curve corresponds to γ -rays from the decay of neutral pions produced by collisions of the relativistic proton component with ambient nuclei. (The curvature of the particle spectra associated with DSA is particularly evident in the synchrotron and IC emission.)

The emission from both NTB and π^0 -decay scales with the ambient density n_0 . As a result, in high density environments such as those encountered in SNR/MC interactions, significant γ -ray emission is expected if the SNR has been an active particle accelerator. For $K_{\text{ep}} \sim 10^{-2}$, as measured locally, the π^0 -decay emission will dominate (see Figure 8), making such γ -ray emission an important probe of the hadronic component of the particles accelerated by the SNR.

An important additional consideration for γ -ray production is the local photon energy density. Contributions from starlight as well as IR emission from local dust can increase the IC emission and change the spectral shape of this component due to the different effective temperatures of these photon components. These contributions are highly dependent upon galactocentric radius (e.g., Strong et al. 2000). Moreover, IR emission produced by the SNRs themselves can contribute significantly to the IC γ -ray emission (e.g., Morlino and Caprioli 2012; Slane et al. 2014).

Modeling of the broadband spectra from such SNRs, in order to ascertain the nature of the γ -ray emission, is complicated and has led to mixed interpretations, making the evidence for ion acceleration controversial in some cases. However, in a growing number of cases, γ -ray emission from some SNRs known to be interacting with MCs seems to clearly require a significant component from pion decay. We discuss emission from several of these sources below.

4.3 Gamma-ray Observations of SNRs

To date, studies have identified γ -ray emission from ~ 25 SNRs, the majority of which are interacting with MCs. Of these, the evidence for energetic hadrons as the source of these γ -rays is compelling for more than 50% of these based on energetic arguments and/or broadband spectral modeling. *Fermi* LAT observations of W51C reveal a spectrum that is consistent with π^0 -decay, with dominant NTB ruled out unless $K_{\text{ep}} \gg 0.01$, and IC emission ruled out on energetic grounds (Abdo et al. 2009). W44 and IC 443 show clear evidence of a kinematic “pion bump” in their spectra, firmly establishing the presence of energetic ions in these remnants (Abdo et al. 2010; Giuliani et al. 2011; Ackermann et al. 2013). Gamma-ray emission from CTB 109 (Figure 4, left) has been detected with the *Fermi* LAT (Castro et al. 2012), and modeling of the broadband emission (Figure 4, upper right) indicates that the γ -ray emission arises from approximately equal contributions from IC scattering and π^0 -decay, a result that is strongly constrained by the observed ionization state of the thermal X-ray emission (Figure 4, lower right).

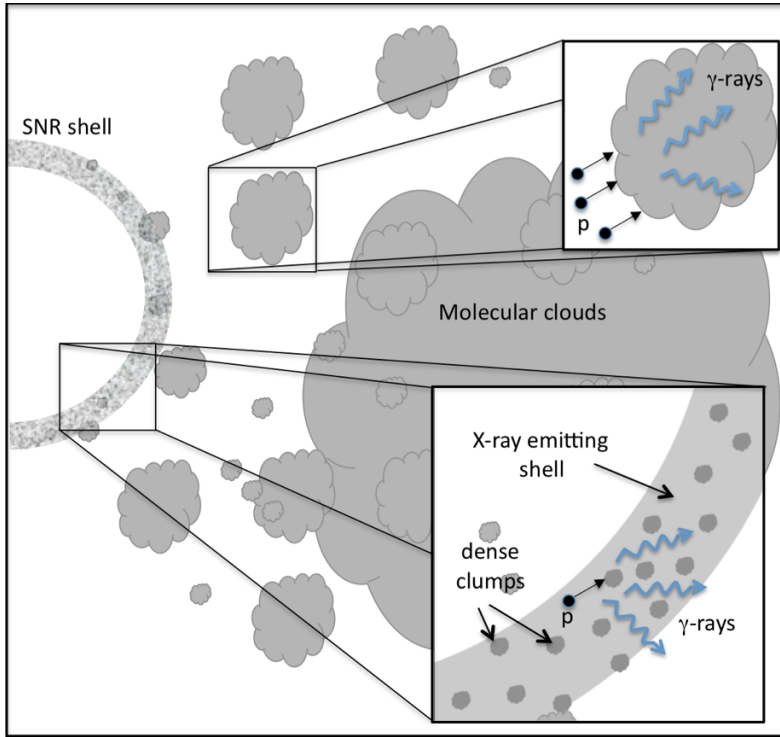


Fig. 9 Schematic diagram of SNR/MC interaction in which postshock region in SNR contains dense clumps within shocked interclump material. The low-density shocked interclump gas emits X-rays. Protons acceleration by the SNR encounter all of gas in the shell, and γ -rays are produced primarily through collisions with the dense clumps.

Castro & Slane (2010) carried out *Fermi* LAT studies of a set of four SNRs (G349.7+0.2, CTB 37A, 3C 391, and G8.7–0.1) known to be interacting with MCs based on observations of hydroxyl (OH) maser emission at 1720 MHz, and showed that all four were sources of GeV γ -ray emission. Based on the assumption that the γ -ray emission is dominated by π^0 -decay produced in the compressed shell of the SNR, they derived a lower limit on the density of the γ -ray emitting material for each remnant, and compared this with the density inferred from X-ray measurements. They found that the density inferred from γ -ray measurements exceeds that from X-ray measurements by a factor of 20 or more. Subsequent studies of W41, MSH 17–39, and G337.7–0.1 (Castro et al. 2013) as well as Kes 79 (Auchettl et al. 2014) reveal γ -ray spectra indicative of hadronic emission, with leptonic scenarios requiring total electron energies in excess of 10^{51} erg or $K_{ep} \gg 0.01$. Similar discrepancies between densities inferred from γ -ray and X-ray measurements are obtained for these sources. The magnetic fields implied by the radio emission in these studies is typically much larger than expected from the compressed ISM, suggesting evidence for the magnetic field amplification expected in efficient particle acceleration in SNR shocks.

A plausible explanation for the observed discrepancy between n_x and n_γ is that these SNRs, by evolving in the presence of MCs, have swept up clumps of dense material. The SNR blast wave for each remnant has presumably evolved primarily through the low-density interclump medium, heating this material to X-ray emitting temperatures and accelerating particles through DSA. The proton component of these accelerated particles then interacts with both the dense clumps and the interclump gas, thus sampling a much higher effective density than that of the X-ray emitting gas (Figure 9). A similar scenario has been proposed by (Inoue et al. 2012) to explain the complete lack of thermal X-ray emission from RX J1713.7–3946, whose observed GeV and TeV γ -ray emission is otherwise required to be dominated by IC emission (Ellison et al. 2010, 2012). Additional modifications of this picture of dense clumps embedded in the SNR shell invokes reacceleration of cosmic rays trapped in the cold molecular material rather than trapped particles in the shell that have been accelerated by the SNR (e.g., Uchiyama et al. 2010).

An alternative scenario that can explain γ -rays from SNR/MC interactions, and also $n_\gamma/n_x \gg 1$, is that of escaping CRs interacting with external MCs (e.g., Gabici et al. 2009). Here, as indicated in Figure 9 (left), there is no connection between n_x and n_γ because the X-rays are produced in the SNR shell while the γ -rays are from the MC. Such a scenario has been suggested to explain the γ -rays from the source MAGIC J0616+225 as the result of energetic particles that have escaped from IC 443 and are interacting with dense clouds (Torres et al. 2008), for example, and discrete TeV sources outside the remnant W28 have been suggested to originate from particles escaping the SNR and interacting with adjacent clouds (Aharonian et al. 2008). The expected γ -ray spectrum in this scenario is complicated, however. Because the escaping particles are distributed around E_{\max} , the resulting π^0 -decay spectrum is peaked at higher energies than that for the shell (Zirakashvili and Ptuskin 2008; Ellison and Bykov 2011). However, because E_{\max} is expected to decrease with time, the time-accumulated spectrum of particles interacting with a remote cloud will depend on the age of the SNR and the energy-dependent diffusion process by which the particles are transported. For simple assumptions about the time evolution and particle diffusion, this could lead to power law (Gabici et al. 2009) or broken power law (Ohira et al. 2011) particle distributions at the remote cloud site. The observed γ -ray spectra from W51C, W28, W44 and IC 443 show distinctly different slopes, leading to questions as to whether these differences are intrinsic to the acceleration or the result of complex evolution, propagation, and interaction with remote clouds.

5 Conclusions

Observations of SNR/MC interactions provide unique information on the distances to SNRs and on the physics of shock/cloud interactions. X-ray observations, in particular, probe the state of the shocked gas and provide diagnostics of the interaction through absorption, ionization, temperature, and general morphology measurements. For SNRs that are, or have been, active particle accelerators, these interactions with dense cloud material can lead to crucial measurements of emission from the hadronic

component of their relativistic particle spectra, providing crucial information on acceleration efficiency, maximum energies, and particle escape in these systems.

Recent studies of γ -ray emission from numerous SNRs demonstrate that those interacting with MCs show strong evidence of relativistic protons. For some, X-ray measurements of the flux or ionization state of the thermal plasma provide constraints that allow us to determine what fraction of the γ -ray emission arises from this hadronic component. For a significant number of the remnants interacting with MCs, the inferred density of the γ -ray-emitting material is considerably higher than that determined from X-ray measurements, suggesting a complex emission environment with dense clumps embedded in hot interclump gas, or perhaps significant γ -ray emission associated with escaping cosmic rays interacting with external clouds. Considerable additional observations and modeling efforts are required to better understand the postshock regions of SNR/MC interactions, as well as the evolution and transport of the escaping particles. Of particular importance are simulations of SNR evolution into dense, cloudy environments to study the formation of clumps in the postshock region, as well as modeling of realistic particle acceleration with escape and energy-dependent diffusion to predict the spectrum of SNR cosmic rays interacting with nearby MCs. Equally important is progress in observations and modeling of supernova ejecta interactions with a complex circumstellar medium formed by the winds of massive stars at the different evolution stages of the massive stars. On the observational side, more sensitive X-ray and γ -ray observations are needed to provide improved spectra of SNRs interacting with MCs. Improved angular resolution at γ -ray energies, such as may be expected in future facilities like CTA, is particularly important. In combination with current studies of plasma instabilities, magnetic field amplification, and the reacceleration of relic cosmic rays, the outlook for reaching a quantitative understanding of the role SNRs play in producing Galactic cosmic rays is extremely positive.

Acknowledgements The authors would like to thank Tom Dame and Herman Lee for important discussions contributing to this paper. We also thank ISSI and its staff for supporting this effort and for creating a stimulating environment for the meeting at which this work was initiated. POS acknowledges support from NASA Contract NAS8-03060. AMB was supported in part by RAS Presidium 21 and OFN 15 programs.

References

- A.A. Abdo, M. Ackermann, M. Ajello, L. Baldini, J. Ballet, et al. Fermi LAT Discovery of Extended Gamma-Ray Emission in the Direction of Supernova Remnant W51C. *ApJ* **706**, 1–6 (2009)
- A.A. Abdo, M. Ackermann, M. Ajello, L. Baldini, J. Ballet, et al. Gamma-Ray Emission from the Shell of Supernova Remnant W44 Revealed by the Fermi LAT. *Science* **327**, 1103 (2010)
- V.A. Acciari, E. Aliu, T. Arlen, T. Aune, M. Bautista, et al. Observation of Extended Very High Energy Emission from the Supernova Remnant IC 443 with VERITAS. *ApJ* **698**, 133–137 (2009). doi:10.1088/0004-637X/698/2/L133
- M. Ackermann, M. Ajello, A. Allafort, L. Baldini, J. Ballet, et al. Detection of the Characteristic Pion-Decay Signature in Supernova Remnants. *Science* **339**, 807–811 (2013)
- F.A. Aharonian, L.O. Drury, H.J. Voelk, GeV/TeV gamma-ray emission from dense molecular clouds overtaken by supernova shells. *A&A* **285**, 645–647 (1994)
- F. Aharonian, A.G. Akhperjanian, A.R. Bazer-Bachi, B. Behera, M. Beilicke, et al. Discovery of very high energy gamma-ray emission coincident with molecular clouds in the W 28 (G6.4-0.1) field. *A&A* **481**, 401–410 (2008). doi:10.1051/0004-6361:20077765

- K. Auchettl, P. Slane, D. Castro, Fermi-LAT Observations of Supernova Remnants Kesteven 79. *ApJ* **783**, 32 (2014). doi:10.1088/0004-637X/783/1/32
- R. Blandford, D. Eichler, Particle acceleration at astrophysical shocks: A theory of cosmic ray origin. *Physics Reports* **154**, 1–75 (1987)
- F. Bocchino, A.M. Bykov, XMM-Newton study of hard X-ray sources in IC 443. *A&A* **400**, 203–211 (2003). doi:10.1051/0004-6361:20021858
- F. Bocchino, M. Miceli, E. Troja, On the metal abundances inside mixed-morphology supernova remnants: the case of IC 443 and G166.0+4.3. *A&A* **498**, 139–145 (2009). doi:10.1051/0004-6361/200810742
- F. Bocchino, A.M. Bykov, Y. Chen, A.M. Krassilchtchikov, K.P. Levenfish, M. Miceli, G.G. Pavlov, Y.A. Uvarov, X. Zhou, A population of isolated hard X-ray sources near the supernova remnant Kes 69. *A&A* **541**, 152 (2012). doi:10.1051/0004-6361/201219005
- C.L. Brogan, D.A. Frail, W.M. Goss, T.H. Troland, OH Zeeman Magnetic Field Detections toward Five Supernova Remnants Using the VLA. *ApJ* **537**, 875–890 (2000). doi:10.1086/309068
- C.L. Brogan, W.M. Goss, T.R. Hunter, A.M.S. Richards, C.J. Chandler, J.S. Lazendic, B.-C. Koo, I.M. Hoffman, M.J. Claussen, OH (1720 MHz) Masers: A Multiwavelength Study of the Interaction between the W51C Supernova Remnant and the W51B Star Forming Region. *ApJ* **771**, 91 (2013). doi:10.1088/0004-637X/771/2/91
- M.G. Burton, T.R. Geballe, P.W.J.L. Brand, A.S. Webster, Shocked molecular hydrogen in the supernova remnant IC 443. *MNRAS* **231**, 617–634 (1988)
- M.G. Burton, C. Braiding, C. Glueck, P. Goldsmith, J. Hawkes, D.J. Hollenbach, C. Kulesa, C.L. Martin, J.L. Pineda, G. Rowell, R. Simon, A.A. Stark, J. Stutzki, N.J.H. Tothill, J.S. Urquhart, C. Walker, A.J. Walsh, M. Wolfire, The Mopra Southern Galactic Plane CO Survey. *PASA* **30**, 44 (2013). doi:10.1017/pasa.2013.22
- A.M. Bykov, X-ray line emission from supernova ejecta fragments. *A&A* **390**, 327–335 (2002). doi:10.1051/0004-6361:20020694
- A.M. Bykov, A.M. Krassilchtchikov, Y.A. Uvarov, H. Bloemen, F. Bocchino, G.M. Dubner, E.B. Giacani, G.G. Pavlov, Isolated X-Ray-Infrared Sources in the Region of Interaction of the Supernova Remnant IC 443 with a Molecular Cloud. *ApJ* **676**, 1050–1063 (2008). doi:10.1086/529117
- A.M. Bykov, M.A. Malkov, J.C. Raymond, A.M. Krassilchtchikov, A.E. Vladimirov, Collisionless Shocks in Partly Ionized Plasma with Cosmic Rays: Microphysics of Non-thermal Components. *Space Sci. Rev.* **178**, 599–632 (2013a). doi:10.1007/s11214-013-9984-7
- A.M. Bykov, A. Brandenburg, M.A. Malkov, S.M. Osipov, Microphysics of Cosmic Ray Driven Plasma Instabilities. *Space Sci. Rev.* (2013b)
- G. Cassam-Chenaï, J.P. Hughes, E.M. Reynoso, C. Badenes, D. Moffett, Morphological Evidence for Azimuthal Variations of the Cosmic-Ray Ion Acceleration at the Blast Wave of SN 1006. *ApJ* **680**, 1180–1197 (2008)
- G. Castelletti, G. Dubner, T. Clarke, N.E. Kassim, High-resolution radio study of SNR IC 443 at low radio frequencies. *A&A* **534**, 21 (2011). doi:10.1051/0004-6361/201016081
- D. Castro, P. Slane, Fermi Large Area Telescope Observations of Supernova Remnants Interacting with Molecular Clouds. *ApJ* **717**, 372–378 (2010)
- D. Castro, P. Slane, D.C. Ellison, D.J. Patnaude, Fermi-LAT Observations and a Broadband Study of Supernova Remnant CTB 109. *ApJ* **756**, 88 (2012). doi:10.1088/0004-637X/756/1/88
- D. Castro, P. Slane, A. Carlton, E. Figueroa-Feliciano, Fermi-LAT Observations of Supernova Remnants Interacting with Molecular Clouds: W41, MSH 17-39, and G337.7-0.1. *ApJ* **774**, 36 (2013)
- Y. Chen, B. Jiang, Multi-wavelength studies on interaction of supernova remnants with molecular clouds. *Scientia Sinica Physica, Mechanica & Astronomica* **43**, 1 (2013)
- Y. Chen, P.O. Slane, ASCA Observations of the Thermal Composite Supernova Remnant 3C 391. *ApJ* **563**, 202–208 (2001). doi:10.1086/323886
- Y. Chen, Y. Su, P.O. Slane, Q.D. Wang, A Chandra ACIS View of the Thermal Composite Supernova Remnant 3C 391. *ApJ* **616**, 885–894 (2004). doi:10.1086/425152
- Y. Chen, B. Jiang, P. Zhou, Y. Su, X. Zhou, H. Li, X. Zhang, Molecular Environments of SNRs. *ArXiv e-prints* (2013)
- R.A. Chevalier, Supernova Remnants in Molecular Clouds. *ApJ* **511**, 798–811 (1999). doi:10.1086/306710
- D.F. Cioffi, C.F. McKee, E. Bertschinger, Dynamics of radiative supernova remnants. *ApJ* **334**, 252–265 (1988). doi:10.1086/166834
- M.J. Claussen, D.A. Frail, W.M. Goss, R.A. Gaume, Polarization Observations of 1720 MHz OH Masers toward the Three Supernova Remnants W28, W44, and IC 443. *ApJ* **489**, 143 (1997).

- doi:10.1086/304784
- F.R. Colomb, G. Dubner, Neutral hydrogen associated with southern supernova remnants. II - Lupus Loop. *A&A* **112**, 141–148 (1982)
- D.P. Cox, The Three-Phase Interstellar Medium Revisited. *ARA&A* **43**, 337–385 (2005). doi:10.1146/annurev.astro.43.072103.150615
- D.P. Cox, R.L. Shelton, W. Maciejewski, R.K. Smith, T. Plewa, A. Pawl, M. Różyczka, Modeling W44 as a Supernova Remnant in a Density Gradient with a Partially Formed Dense Shell and Thermal Conduction in the Hot Interior. I. The Analytical Model. *ApJ* **524**, 179–191 (1999)
- T.M. Dame, D. Hartmann, P. Thaddeus, The Milky Way in Molecular Clouds: A New Complete CO Survey. *ApJ* **547**, 792–813 (2001). doi:10.1086/318388
- L.K. Denoyer, M.A. Frerking, Some new results on shock chemistry in IC 443. *ApJ* **246**, 37–40 (1981). doi:10.1086/183548
- G.M. Dubner, F.R. Colomb, E.B. Giacani, 1410 MHz continuum and H I line observations towards the SNR G296.5 + 10.0 and nearby sources - Evidences of two SNRs tunneling through the interstellar medium. *AJ* **91**, 343–353 (1986). doi:10.1086/114015
- G.M. Dubner, M. Holdaway, W.M. Goss, I.F. Mirabel, A High-Resolution Radio Study of the W50-SS 433 System and the Surrounding Medium. *AJ* **116**, 1842–1855 (1998a). doi:10.1086/300537
- G.M. Dubner, A.J. Green, W.M. Goss, D.C.-J. Bock, E. Giacani, Neutral Hydrogen in the Direction of the VELA Supernova Remnant. *AJ* **116**, 813–822 (1998b). doi:10.1086/300466
- G.M. Dubner, E.B. Giacani, W.M. Goss, A.J. Green, L.-Å. Nyman, The neutral gas environment of the young supernova remnant SN 1006 (G327.6+14.6). *A&A* **387**, 1047–1056 (2002). doi:10.1051/0004-6361:20020365
- D.C. Ellison, A.M. Bykov, Gamma-ray Emission of Accelerated Particles Escaping a Supernova Remnant in a Molecular Cloud. *ApJ* **731**, 87 (2011). doi:10.1088/0004-637X/731/2/87
- D.C. Ellison, E. Moebius, G. Paschmann, Particle injection and acceleration at earth's bow shock - Comparison of upstream and downstream events. *ApJ* **352**, 376–394 (1990)
- D.C. Ellison, J. Giacalone, D. Burgess, S.J. Schwartz, Simulations of particle acceleration in parallel shocks: Direct comparison between Monte Carlo and one-dimensional hybrid codes. *J. Geophys. Res.* **98**, 21085 (1993)
- D.C. Ellison, D.J. Patnaude, P. Slane, J. Raymond, Efficient Cosmic Ray Acceleration, Hydrodynamics, and Self-Consistent Thermal X-Ray Emission Applied to Supernova Remnant RX J1713.7–3946. *ApJ* **712**, 287–293 (2010)
- D.C. Ellison, P. Slane, D.J. Patnaude, A.M. Bykov, Core-collapse Model of Broadband Emission from SNR RX J1713.7–3946 with Thermal X-Rays and Gamma Rays from Escaping Cosmic Rays. *ApJ* **744**, 39 (2012)
- R.A. Fesen, R.P. Kirshner, Spectrophotometry of the supernova remnant IC 443. *ApJ* **242**, 1023–1040 (1980). doi:10.1086/158534
- D.A. Frail, G.F. Mitchell, OH (1720 MHz) Masers as Signposts of Molecular Shocks. *ApJ* **508**, 690–695 (1998). doi:10.1086/306452
- D.A. Frail, W.M. Goss, V.I. Slysh, Shock-excited maser emission from the supernova remnant W28. *ApJ* **424**, 111–113 (1994)
- D.A. Frail, W.M. Goss, E.M. Reynoso, E.B. Giacani, A.J. Green, R. Otrupcek, A Survey for OH (1720 MHz) Maser Emission Toward Supernova Remnants. *AJ* **111**, 1651 (1996)
- K.É. Gabányi, G. Dubner, E. Giacani, Z. Paragi, S. Frey, Y. Pidopryhora, Very Long Baseline Interferometry Search for the Radio Counterpart of HESS J1943+213. *ApJ* **762**, 63 (2013). doi:10.1088/0004-637X/762/1/63
- S. Gabici, F.A. Aharonian, S. Casanova, Broad-band non-thermal emission from molecular clouds illuminated by cosmic rays from nearby supernova remnants. *MNRAS* **396**, 1629–1639 (2009). doi:10.1111/j.1365-2966.2009.14832.x
- A. Giuliani, M. Cardillo, M. Tavani, Y. Fukui, S. Yoshiike, et al. Neutral Pion Emission from Accelerated Protons in the Supernova Remnant W44. *ApJ* **742**, 30 (2011)
- O. Gnat, A. Sternberg, Metal-Absorption Column Densities in Fast Radiative Shocks. *ApJ* **693**, 1514–1542 (2009). doi:10.1088/0004-637X/693/2/1514
- J.R. Graham, N.A. Levenson, J.J. Hester, J.C. Raymond, R. Petre, An X-ray and optical study of the interaction of the Cygnus Loop supernova remnant with an interstellar cloud. *ApJ* **444**, 787–795 (1995). doi:10.1086/175651
- A.J. Green, D.A. Frail, W.M. Goss, R. Otrupcek, Continuation of a survey of OH (1720 MHz) Maser Emission Towards Supernova Remnants. *AJ* **114**, 2058 (1997)

- Y. Hanabata, M. Sawada, H. Katagiri, A. Bamba, Y. Fukazawa, X-Ray Observations of the W 51 Complex with Suzaku. *PASJ* **65**, 42 (2013)
- J.W. Hewitt, F. Yusef-Zadeh, M. Wardle, A Survey of Hydroxyl toward Supernova Remnants: Evidence for Extended 1720 MHz Maser Emission. *ApJ* **683**, 189–206 (2008). doi:10.1086/588652
- M.H. Heyer, C. Brunt, R.L. Snell, J.E. Howe, F.P. Schloerb, J.M. Carpenter, The Five College Radio Astronomy Observatory CO Survey of the Outer Galaxy. *ApJS* **115**, 241 (1998). doi:10.1086/313086
- I.M. Hoffman, W.M. Goss, C.L. Brogan, M.J. Claussen, The OH (1720 MHz) Supernova Remnant Masers in W44: MERLIN and VLBA Polarization Observations. *ApJ* **627**, 803–812 (2005). doi:10.1086/430419
- D. Hollenbach, C.F. McKee, Molecule formation and infrared emission in fast interstellar shocks. III - Results for J shocks in molecular clouds. *ApJ* **342**, 306–336 (1989). doi:10.1086/167595
- Y.-L. Huang, P. Thaddeus, Molecular clouds and supernova remnants in the outer galaxy. *ApJ* **309**, 804–821 (1986). doi:10.1086/164649
- T. Inoue, R. Yamazaki, S.-i. Inutsuka, Y. Fukui, Toward Understanding the Cosmic-Ray Acceleration at Young Supernova Remnants Interacting with Interstellar Clouds: Possible Applications to RX J1713.7-3946. *ApJ* **744**, 71 (2012)
- J.M. Jackson, J.M. Rathborne, R.Y. Shah, R. Simon, T.M. Bania, D.P. Clemens, E.T. Chambers, A.M. Johnson, M. Dormody, R. Lavoie, M.H. Heyer, The Boston University-Five College Radio Astronomy Observatory Galactic Ring Survey. *ApJS* **163**, 145–159 (2006). doi:10.1086/500091
- B. Jiang, Y. Chen, J. Wang, Y. Su, X. Zhou, S. Safi-Harb, T. DeLaney, Cavity of Molecular Gas Associated with Supernova Remnant 3C 397. *ApJ* **712**, 1147–1156 (2010)
- S. Katsuda, R. Petre, J.P. Hughes, U. Hwang, H. Yamaguchi, A. Hayato, K. Mori, H. Tsunemi, X-ray Measured Dynamics of Tycho's Supernova Remnant. *ApJ* **709**, 1387–1395 (2010)
- M.T. Kawasaki, M. Ozaki, F. Nagase, K. Masai, M. Ishida, R. Petre, ASCA Observations of the Supernova Remnant IC 443: Thermal Structure and Detection of Overionized Plasma. *ApJ* **572**, 897–905 (2002). doi:10.1086/340383
- T. Kokusho, T. Nagayama, H. Kaneda, D. Ishihara, H.-G. Lee, T. Onaka, Large-area [Fe II] Line Mapping of the Supernova Remnant IC 443 with the IRSF/SIRIUS. *ApJ* **768**, 8 (2013). doi:10.1088/2041-8205/768/1/L8
- B.-C. Koo, J.-H. Kang, N.M. McClure-Griffiths, HI 21 cm Emission Line Study of Southern Galactic Supernova Remnants. *Journal of Korean Astronomical Society* **37**, 61–77 (2004)
- B.-C. Koo, J.-J. Lee, F.D. Seward, An ASCA Study of the W51 Complex. *AJ* **123**, 1629–1638 (2002). doi:10.1086/339179
- B.-C. Koo, J.-J. Lee, F.D. Seward, D.-S. Moon, Chandra Observations of the W51C Supernova Remnant. *ApJ* **633**, 946–952 (2005). doi:10.1086/491468
- R. Kothes, B. Uyaniker, A. Yar, The Distance to Supernova Remnant CTB 109 Deduced from Its Environment. *ApJ* **576**, 169–175 (2002). doi:10.1086/341545
- J.S. Lazendic, P.O. Slane, Enhanced Abundances in Three Large-Diameter Mixed-Morphology Supernova Remnants. *ApJ* **647**, 350–366 (2006). doi:10.1086/505380
- D.A. Leahy, W.W. Tian, The distance of the SNR Kes 75 and PWN PSR J1846-0258 system. *A&A* **480**, 25–28 (2008). doi:10.1051/0004-6361/20079149
- J.-J. Lee, B.-C. Koo, M.S. Yun, S. Stanimirović, C. Heiles, M. Heyer, A 21 cm Spectral and Continuum Study of IC 443 Using the Very Large Array and the Arecibo Telescope. *AJ* **135**, 796–808 (2008). doi:10.1088/0004-6256/135/3/796
- J.-J. Lee, B.-C. Koo, R.L. Snell, M.S. Yun, M.H. Heyer, M.G. Burton, Identification of Ambient Molecular Clouds Associated with Galactic Supernova Remnant IC 443. *ApJ* **749**, 34 (2012). doi:10.1088/0004-637X/749/1/34
- N.A. Levenson, J.R. Graham, S.L. Snowden, The Cygnus Loop: A Soft-shelled Supernova Remnant. *ApJ* **526**, 874–880 (1999)
- P. Lockett, E. Gauthier, M. Elitzur, OH 1720 Megahertz Masers in Supernova Remnants: C-Shock Indicators. *ApJ* **511**, 235–241 (1999)
- L.A. Lopez, E. Ramirez-Ruiz, C. Badenes, D. Huppenkothen, T.E. Jeltema, D.A. Pooley, Typing Supernova Remnants Using X-Ray Line Emission Morphologies. *ApJ* **706**, 106–109 (2009)
- L.A. Lopez, S. Pearson, E. Ramirez-Ruiz, D. Castro, H. Yamaguchi, P.O. Slane, R.K. Smith, Unraveling the Origin of Overionized Plasma in the Galactic Supernova Remnant W49B. *ApJ* **777**, 145 (2013). doi:10.1088/0004-637X/777/2/145
- M.A. Malkov, L.O. Drury, Nonlinear theory of diffusive acceleration of particles by shock waves. *Reports of Progress in Physics* **64**, 429–481 (2001a)

- M.A. Malkov, L.O. Drury, Nonlinear theory of diffusive acceleration of particles by shock waves. *Reports of Progress in Physics* **64**, 429–481 (2001b)
- R.L. McEntaffer, T. Brantseg, Chandra Imaging and Spectroscopy of the Eastern XA Region of the Cygnus Loop Supernova Remnant. *ApJ* **730**, 99 (2011). doi:10.1088/0004-637X/730/2/99
- M. Miceli, F. Bocchino, A. Decourchelle, J. Ballet, F. Reale, Spatial identification of the overionized plasma in W49B. *A&A* **514**, 2 (2010). doi:10.1051/0004-6361/200913713
- M. Miceli, F. Acero, G. Dubner, A. Decourchelle, S. Orlando, F. Bocchino, Shock-Cloud Interaction and Particle Acceleration in the Southwestern Limb of SN 1006. *ApJ* **782**, 33 (2014). doi:10.1088/2041-8205/782/2/L33
- T.J. Moriya, Progenitors of Recombining Supernova Remnants. *ApJ* **750**, 13 (2012)
- G. Morlino, D. Caprioli, Strong evidence for hadron acceleration in Tycho's supernova remnant. *A&A* **538**, 81 (2012)
- R. Morrison, D. McCammon, Interstellar photoelectric absorption cross sections, 0.03–10 keV. *ApJ* **270**, 119–122 (1983). doi:10.1086/161102
- R. Nakamura, A. Bamba, M. Ishida, R. Yamazaki, K. Tatematsu, K. Kohri, G. Pühlhofer, S.J. Wagner, M. Sawada, X-ray Spectroscopy of the Mixed Morphology Supernova Remnant W28 with XMM-Newton. *ArXiv e-prints* (2014)
- Y. Ohira, K. Murase, R. Yamazaki, Gamma-rays from molecular clouds illuminated by cosmic rays escaping from interacting supernova remnants. *MNRAS* **410**, 1577–1582 (2011). doi:10.1111/j.1365-2966.2010.17539.x
- E. Oliva, D. Lutz, S. Drapatz, A.F.M. Moorwood, ISO-SWS spectroscopy of IC443 and the origin of the IRAS 12 and 25 MU M emission from radiative supernova remnants. *A&A* **341**, 75–78 (1999)
- S. Orlando, F. Bocchino, M. Miceli, X. Zhou, F. Reale, G. Peres, Observability and diagnostics in the X-ray band of shock-cloud interactions in supernova remnants. *A&A* **514**, 29 (2010). doi:10.1051/0004-6361/200913801
- M. Ozawa, K. Koyama, H. Yamaguchi, K. Masai, T. Tamagawa, Suzaku Discovery of the Strong Radiative Recombination Continuum of Iron from the Supernova Remnant W49B. *ApJ* **706**, 71–75 (2009). doi:10.1088/0004-637X/706/1/L71
- T.G. Pannuti, J. Rho, K.J. Borkowski, P.B. Cameron, Mixed-morphology Supernova Remnants in X-rays: Isothermal Plasma in HB21 and Probable Oxygen-rich Ejecta in CTB 1. *AJ* **140**, 1787–1805 (2010). doi:10.1088/0004-6256/140/6/1787
- G. Park, B.-C. Koo, S.J. Gibson, J.-h. Kang, D.C. Lane, K.A. Douglas, J.E.G. Peek, E.J. Korpela, C. Heiles, J.H. Newton, HI Shells and Supershells in the I-GALFA HI 21 cm Line Survey. I. Fast-expanding HI Shells Associated with Supernova Remnants. *ApJ* **777**, 14 (2013). doi:10.1088/0004-637X/777/1/14
- D.J. Patnaude, R.A. Fesen, Small-Scale X-Ray Variability in the Cassiopeia A Supernova Remnant. *AJ* **133**, 147–153 (2007). doi:10.1086/509571
- J.L. Pineda, W.D. Langer, T. Velusamy, P.F. Goldsmith, A Herschel [C ii] Galactic plane survey. I. The global distribution of ISM gas components. *A&A* **554**, 103 (2013). doi:10.1051/0004-6361/201321188
- J.C. Raymond, Shock waves in the interstellar medium. *ApJS* **39**, 1–27 (1979). doi:10.1086/190562
- W.T. Reach, J. Rho, Excitation and Disruption of a Giant Molecular Cloud by the Supernova Remnant 3C 391. *ApJ* **511**, 836–846 (1999). doi:10.1086/306703
- W.T. Reach, J. Rho, T.H. Jarrett, Shocked Molecular Gas in the Supernova Remnants W28 and W44: Near-Infrared and Millimeter-Wave Observations. *ApJ* **618**, 297–320 (2005). doi:10.1086/425855
- W.T. Reach, J. Rho, A. Tappe, T.G. Pannuti, C.L. Brogan, E.B. Churchwell, M.R. Meade, B. Babler, R. Indebetouw, B.A. Whitney, A Spitzer Space Telescope Infrared Survey of Supernova Remnants in the Inner Galaxy. *AJ* **131**, 1479–1500 (2006). doi:10.1086/499306
- E.M. Reynoso, P.F. Velázquez, G.M. Dubner, W.M. Goss, The Environs of Tycho's Supernova Remnant Explored through the HI 21 Centimeter Line. *AJ* **117**, 1827–1833 (1999). doi:10.1086/300814
- E.M. Reynoso, A.J. Green, S. Johnston, G.M. Dubner, E.B. Giacani, W.M. Goss, Observations of the neutral hydrogen surrounding the radio-quiet neutron star RX J0822-4300 in Puppis A. *MNRAS* **345**, 671–677 (2003). doi:10.1046/j.1365-8711.2003.06978.x
- J. Rho, T.H. Jarrett, R.M. Cutri, W.T. Reach, Near-Infrared Imaging and [O I] Spectroscopy of IC 443 using Two Micron All Sky Survey and Infrared Space Observatory. *ApJ* **547**, 885–898 (2001). doi:10.1086/318398
- M. Sasaki, C. Heinitz, G. Warth, G. Pühlhofer, XMM-Newton observation of the Galactic supernova remnant W51C (G49.1-0.1). *ArXiv e-prints* (2014)
- M. Sawada, K. Koyama, X-Ray Observations of the Supernova Remnant W28 with Suzaku. I. Spectral

- Study of the Recombining Plasma. *PASJ* **64**, 81 (2012)
- M. Seta, T. Hasegawa, T.M. Dame, S. Sakamoto, T. Oka, T. Handa, M. Hayashi, J.-I. Morino, K. Sorai, K.S. Usuda, Enhanced CO $J = 2-1/J = 1-0$ Ratio as a Marker of Supernova Remnant-Molecular Cloud Interactions: The Cases of W44 and IC 443. *ApJ* **505**, 286–298 (1998). doi:10.1086/306141
- R.L. Shelton, K.D. Kuntz, R. Petre, Chandra Observations and Models of the Mixed-Morphology Supernova Remnant W44: Global Trends. *ApJ* **611**, 906–918 (2004). doi:10.1086/422352
- R.L. Shelton, D.P. Cox, W. Maciejewski, R.K. Smith, T. Plewa, A. Pawl, M. Różyczka, Modeling W44 as a Supernova Remnant in a Density Gradient with a Partially Formed Dense Shell and Thermal Conduction in the Hot Interior. II. The Hydrodynamic Models. *ApJ* **524**, 192–212 (1999)
- L. Sironi, A. Spitkovsky, J. Arons, The Maximum Energy of Accelerated Particles in Relativistic Collisionless Shocks. *ApJ* **771**, 54 (2013)
- P. Slane, R.K. Smith, J.P. Hughes, R. Petre, An X-Ray Study of the Supernova Remnant G290.1-0.8. *ApJ* **564**, 284–290 (2002)
- P. Slane, S.-H. Lee, D.C. Ellison, D.J. Patnaude, J.P. Hughes, K.A. Eriksen, D. Castro, S. Nagataki, A CR-hydro-NEI Model of the Structure and Broadband Emission from Tycho's SNR. *ApJ* **783**, 33–42 (2014)
- R.L. Snell, D. Hollenbach, J.E. Howe, D.A. Neufeld, M.J. Kaufman, G.J. Melnick, E.A. Bergin, Z. Wang, Detection of Water in the Shocked Gas Associated with IC 443: Constraints on Shock Models. *ApJ* **620**, 758–773 (2005). doi:10.1086/427231
- A.W. Strong, I.V. Moskalenko, O. Reimer, Diffuse Continuum Gamma Rays from the Galaxy. *ApJ* **537**, 763–784 (2000). doi:10.1086/309038
- D.F. Torres, A.Y. Rodriguez Marrero, E. de Cea Del Pozo, MAGIC J0616+225 as delayed TeV emission of cosmic rays diffusing from the supernova remnant IC 443. *MNRAS* **387**, 59–63 (2008). doi:10.1111/j.1745-3933.2008.00485.x
- E. Troja, F. Bocchino, M. Miceli, F. Reale, XMM-Newton observations of the supernova remnant IC 443. II. Evidence of stellar ejecta in the inner regions. *A&A* **485**, 777–785 (2008). doi:10.1051/0004-6361:20079123
- H. Uchida, K. Koyama, H. Yamaguchi, M. Sawada, T. Ohnishi, T.G. Tsuru, T. Tanaka, S. Yoshiike, Y. Fukui, Recombining Plasma and Hard X-Ray Filament in the Mixed-Morphology Supernova Remnant W 44. *PASJ* **64**, 141 (2012)
- Y. Uchiyama, F.A. Aharonian, Fast Variability of Nonthermal X-Ray Emission in Cassiopeia A: Probing Electron Acceleration in Reverse-Shocked Ejecta. *ApJ* **677**, 105–108 (2008). doi:10.1086/588190
- Y. Uchiyama, F.A. Aharonian, T. Tanaka, T. Takahashi, Y. Maeda, Extremely fast acceleration of cosmic rays in a supernova remnant. *Nature* **449**, 576–578 (2007). doi:10.1038/nature06210
- Y. Uchiyama, R.D. Blandford, S. Funk, H. Tajima, T. Tanaka, Gamma-ray Emission from Crushed Clouds in Supernova Remnants. *ApJ* **723**, 122–126 (2010). doi:10.1088/2041-8205/723/1/L122
- E.F. van Dishoeck, D.J. Jansen, T.G. Phillips, Submillimeter observations of the shocked molecular gas associated with the supernova remnant IC 443. *A&A* **279**, 541–566 (1993)
- P.F. Velázquez, G.M. Dubner, W.M. Goss, A.J. Green, Investigation of the Large-scale Neutral Hydrogen near the Supernova Remnant W28. *AJ* **124**, 2145–2151 (2002). doi:10.1086/342936
- J. Vink, Supernova remnants: the X-ray perspective. *A&A Rev.* **20**, 49 (2012). doi:10.1007/s00159-011-0049-1
- Z. Wang, N.Z. Scoville, Strongly shocked interstellar gas in IC 443. I - High-resolution molecular observations. *ApJ* **386**, 158–169 (1992). doi:10.1086/171001
- M. Wardle, Enhanced OH in C-Type Shock Waves in Molecular Clouds. *ApJ* **525**, 101–104 (1999)
- G.J. White, R. Rainey, S.S. Hayashi, N. Kaifu, Molecular line observations of IC 443 - The interaction of a molecular cloud and an interstellar shock. *A&A* **173**, 337–346 (1987)
- R.L. White, K.S. Long, Supernova remnant evolution in an interstellar medium with evaporating clouds. *ApJ* **373**, 543–555 (1991)
- B.J. Williams, K.J. Borkowski, P. Ghavamian, J.W. Hewitt, S.A. Mao, R. Petre, S.P. Reynolds, J.M. Blondin, Azimuthal Density Variations around the Rim of Tycho's Supernova Remnant. *ApJ* **770**, 129 (2013)
- P.F. Winkler, B.J. Williams, S.P. Reynolds, R. Petre, K.S. Long, S. Katsuda, U. Hwang, A High-resolution X-Ray and Optical Study of SN1006: Asymmetric Expansion and Small-scale Structure in a Type Ia Supernova Remnant. *ApJ* **781**, 65 (2014). doi:10.1088/0004-637X/781/2/65
- H. Yamaguchi, M. Ozawa, K. Koyama, K. Masai, J.S. Hiraga, M. Ozaki, D. Yonetoku, Discovery of Strong Radiative Recombination Continua from the Supernova Remnant IC 443 with Suzaku. *ApJ* **705**, 6–9 (2009). doi:10.1088/0004-637X/705/1/L6

-
- H. Yamaguchi, M. Tanaka, K. Maeda, P.O. Slane, A. Foster, R.K. Smith, S. Katsuda, R. Yoshii, Elemental Abundances in the Possible Type Ia Supernova Remnant G344.7-0.1. *ApJ* **749**, 137 (2012). doi:10.1088/0004-637X/749/2/137
- Z. Zhang, Y. Gao, J. Wang, CO observation of SNR IC 443. *Science in China: Physics, Mechanics and Astronomy* **53**, 1357–1369 (2010). doi:10.1007/s11433-010-4010-5
- V.N. Zirakashvili, V.S. Ptuskin, Diffusive Shock Acceleration with Magnetic Amplification by Nonresonant Streaming Instability in Supernova Remnants. *ApJ* **678**, 939–949 (2008). doi:10.1086/529580